JOURNAL OF COMPUTATIONAL PHYSICS 81, 151–168 (1989)

Performance and Optimization of Direct Implicit Particle Simulation*

BRUCE I. COHEN, A. BRUCE LANGDON, AND DENNIS W. HEWETT

Lawrence Livermore National Laboratory, University of California, Livermore, California 94550

AND

RICHARD J. PROCASSINI

Department of Nuclear Engineering and Electronics Research Laboratory, Univeristy of California, Berkeley, California 94720

Received November 30, 1987; revised May 10, 1988

Performance characteristics obtained from particle simulations using the direct implicit method are presented. Parameter studies of simulation behavior for an expanding plasma slab have been made determining code performance as functions of $\omega_{pe}\,\Delta t$ and $\Delta x/\lambda_{De}$, where ω_{pe} is the plasma frequency, λ_{De} is the electron Debye length, Δt is the time step, and Δx is the grid spacing. A range of time steps $\omega_{pe}\,\Delta t \leqslant 200$ and mesh sizes $\Delta x/\lambda_{De} \leqslant 100$ were explored. Accurate results for low-frequency phenomena resolved by the time step can be obtained without limit on $\omega_{pe}\,\Delta t$ in this range (and higher) with a careful choice of algorithms. This choice of algorithms defeats a potential nonlinear instability that occurs when $(\omega_{pe}\,\Delta t)^2$ exceeds the number of particles per cell.

1. INTRODUCTION

Implicit time integration schemes allow for the use of larger time steps than conventional explicit methods, thereby extending the applicability of kinetic particle simulation methods. This paper describes a study of the performance and optimization of direct implicit schemes, which are used to follow the trajectories of charged

0021-9991/89 $3.00

particles in an electrostatic, particle-in-cell plasma simulation code. One of the principal goals of this study is the optimization of direct implicit algorithms that are suitable (i.e., efficient, robust, and accurate) for implementation in both 1- and 2-dimensional applications. The time differencing schemes that are studied were developed and analyzed by Langdon [1], and by Cohen, Langdon, and Friedman [2]. Some of the spatial differencing issues were introduced by Langdon, Cohen, and Friedman [3]. The direct implicit method that was used for this study is an alternative to the implicit moment-equation method developed by Mason [4] and Denavit [5].

The organization of this paper is as follows: Section 2 presents the formulation of two time differencing schemes, as well as the incorporation of these schemes into the particle simulation code. Section 3 presents the results of a numerical stability study of these schemes. This study is based upon the energy conservation, or lack thereof, of a freely expanding plasma slab in various regions of $\omega_{pe}\,\Delta t$, $\Delta x/\lambda_{De}$ parameter space, where ω_{pe} is the electron plasma frequence, λ_{De} is the electron Debye length, Δt is the time step, and Δx is the grid spacing. Section 4 discusses avoiding a nonlinear numerical instability when $(\omega_{pe}\,\Delta t)^2$ exceeds the number of particles per cell. Finally, Section 5 summarizes the results of this study. The experience acquired in this study leads to a choice of algorithms and operating parameters for use in 1- and 2-dimensional applications that is efficient, robust, and accurate.

2. The Direct Implicit Electrostatic Particle Code

2.1. *Direct Implicit Time Integration*

The two implicit time integration schemes that were used for this study were chosen for their desirable properties. The most important of these are (i) the relaxation of $\omega\,\Delta t$ constraints on the stability of the method, (ii) strong damping of high-frequency modes for which $\omega\,\Delta t \gtrsim 1$, and (iii) the second-order accuracy of the methods in the simulation of low-frequency phenomena for which $\omega\,\Delta t \lesssim 1$. These properties were originally studied through the normal-mode analysis of an electrostatic, cold-plasma oscillation in which the electrons undergo simple-harmonic oscillations [2]. The present study deals with one scheme from each of the C and D classes of schemes that are discussed in [2]. We now briefly review the description of the C_1 and D_1 schemes. The "optimized C_1 scheme" is given by

$$\mathbf{x}_{n+1} = \mathbf{x}'_{n+1} + (c_0\mathbf{a}_{n+1} + c_1\mathbf{a}_n) \tag{1a}$$

$$\frac{\mathbf{x}'_{n+1} - 2\mathbf{x}'_n + \mathbf{x}'_{n-1}}{\Delta x^2} = \mathbf{a}_n \tag{1b}$$

with $c_0 = 0.302$ and $c_1 = 0.04$, where $\mathbf{x}$ is the particle displacement, $\mathbf{x}'$ is the leapfrog

displacement, and **a** is the acceleration.[1] The subscripts indicate the time step level of the variable. The "D_1 scheme" is given by

$$\frac{\mathbf{v}_{n+1/2}-\mathbf{v}_{n-1/2}}{\Delta t}=\frac{1}{2}\mathbf{a}_{n+1}+\frac{\mathbf{v}_{n-1/2}-\mathbf{v}_{n-3/2}}{2\Delta t}, \tag{2}$$

$$\frac{\mathbf{x}_{n+1}-\mathbf{x}_n}{\Delta t}=\mathbf{v}_{n+1/2}, \tag{3}$$

where **v** is the particle velocity.

2.2. *General Results and Properties*

It was shown in [2] that relaxation of the $\omega_{pe}\,\Delta t$ stability constraint in plasma simulation required the use of an implicit time integration scheme. This means that temporal resolution of the plasma frequency is forfeited to simulate lower frequency phenomena efficiently. This is particularly useful if the phenomenon of interest for the simulation is on a much slower time scale than that of plasma oscillations. Therefore, a time step that encompasses several plasma oscillation periods may be used in long time-scale simulations while the scheme remains numerically stable. The coefficients that are used in the time integration schemes determine the degree of implicitness, the degree of high-frequency mode dissipation, and the stability of the scheme. When $\omega_0\,\Delta t \gg 1$, the high-frequency oscillations cannot be represented, even though the scheme remains stable. Therefore, the scheme should damp out these modes, while not affecting the low-frequency modes which are of interest. The $|z|$ for the least damped simple-harmonic oscillator normal mode is plotted as a function of $\omega_0^2\,\Delta t^2$, for both the C_1 and D_1 schemes in Fig. 1. The figure shows that the damping for the D_1 scheme is stronger, and begins at smaller values of $\omega_0\,\Delta t$, than that for the C_1 scheme. This is due to the fact that the only acceleration used in (2) is $\mathbf{a}_{n+1}$, indicating that the D_1 scheme attempts to force charge neutrality in only one time step as $\Delta t \to \infty$. In contrast, the C_1 scheme uses acceleration data from several previous time steps. In 1-dimensional implementations, the C_1 scheme requires that one more particle-length array be stored than does the D_1 scheme. The accuracy of the two schemes at low frequencies was discussed in [2]. The weak damping of low-frequency oscillations indicated in Fig. 1 yields high accuracy simulations in the "explicit" regime $\omega_0\,\Delta t < 1$.

2.3. *Electrostatic Field Equations*

In general, the direct implicit time integration schemes give the new particle position as

$$\mathbf{x}_{n+1}=\beta\,\Delta t^2\mathbf{a}_{n+1}+\tilde{\mathbf{x}}, \tag{4}$$

[1] For multistep schemes of the form (1a)–(1b), and for $\omega_0\,\Delta t \to \infty$, P.-A. Raviart has shown analytically that the three normal modes have equal damping, given by $|z| = |\exp(-i\omega\,\Delta t)| = \frac{1}{2}$, when $8c_1 = c_0 = 8/27$. These values agree with those obtained by Cohen *et al.* [3] that minimized the value of $|z|$ for the least stable root, to within the accuracy of their numerical determination.

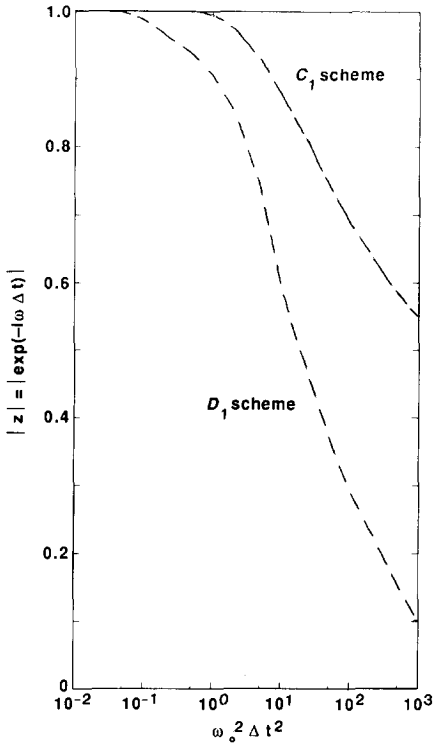

FIG. 1. The absolute value of $|z| = |\exp(-i\omega \Delta t)|$ of the least damped simple-harmonic oscillator normal mode versus $\omega_0^2 \Delta t^2$ in the C_1 scheme (dashed line) and the D_1 scheme (dashed-dotted line).

where $0 < \beta \lesssim 1$ is a constant of the time integration scheme and $\tilde{\mathbf{x}}$ is the explicitly computable "free-streaming" particle position, which is independent of $\mathbf{a}_{n+1}$. In an electrostatic code [3], $\mathbf{a}_{n+1}$ is due only to $\mathbf{E}_{n+1}$.

The new position $\mathbf{x}_{n+1}$ may be thought of as the explicitly computable position $\tilde{\mathbf{x}}$ plus a displacement $\delta\mathbf{x} = \beta \Delta t^2 \mathbf{a}_{n+1}$. The charge density is then taken as the sum of $\tilde{\rho}$ depending on the positions of $\tilde{\mathbf{x}}$, plus a linearized correction term due to the displacing of the particles by the amount $\delta\mathbf{x} = \mathbf{x}_{n+1} - \tilde{\mathbf{x}}$, which is equal to

$$\delta\rho = -\nabla \cdot [\tilde{\rho}(\mathbf{x})\, \delta\mathbf{x}(\mathbf{x})]. \tag{5}$$

The linearized displacement term

$$\delta\mathbf{x}(\mathbf{x}) \cong \beta \Delta t^2 q \mathbf{E}_{n+1}/m \tag{6}$$

then gives

$$\delta\rho(\mathbf{x}) = -\nabla \cdot [\chi(\mathbf{x})\, \mathbf{E}_{n+1}], \tag{7}$$

where the implicit susceptibility is defined by

$$\chi(\mathbf{x}) = \beta[q\tilde{\rho}(\mathbf{x})/m] = \beta(\omega_p \Delta t)^2. \tag{8}$$

(These expressions have been generalized to the relativistic case [6] and implemented in our computer code TESS, which stands for tandem experiment simulation studies). Poisson's equation is modified by the addition of this susceptibility to become, in rationalized cgs units

$$\nabla \cdot \mathbf{E}_{n+1} = \tilde{\rho} - \nabla \cdot (\chi \mathbf{E}_{n+1}) \tag{9}$$

or

$$-\nabla \cdot [1+\chi] \nabla \phi_{n+1} = \tilde{\rho}. \tag{10}$$

This form of the field equation depends only upon the particle position $\mathbf{x}_{n+1}$, as opposed to the implicit moment-equation method which also requires particle velocity information [4, 5].

The TESS code uses a simplified finite difference form of (10), which in the absence of local spatial smoothing is given by [3],

$$-[1+\chi_{j+1/2}](\phi_{j+1} - \phi_j) + [1+\chi_{j-1/2}](\phi_j - \phi_{j-1}) = \tilde{\rho}_j \Delta x^2, \tag{11}$$

where

$$\chi_{j\pm 1/2} = (\chi_j + \chi_{j\pm 1})/2 \tag{12}$$

is a midpoint implicit susceptibility. This choice is motivated by the consideration of nonlinear stability described in Section IV. Other choices for χ_j have been used, including the maximum of the adjacent gridpoint values of χ. In the simulation of long time scale phenomena, it is desirable to have a value of $\omega_p^2 \Delta t^2 \gg 1$, which means that $[1+\chi] \gg 1$, such that the field equation is substantially different from Poisson's equation, which is the explicit limit of (10) for $\omega_p^2 \Delta t^2 \ll 1$.

The analogous field equations for the 2-dimensional implicit electromagnetic particle code AVANTI are similar in philosophy, but considerably more complicated in form [7]. This complexity strongly motivates a simplified spatial differencing scheme to streamline the resulting matrix equations. The stability and accuracy of simplified differencing is studied here in an electrostatic implementation.

3. Direct Implicit Methods Performance Study

The performance of the C_1 and D_1 time integration schemes, as a function of location in $\omega_{pe} \Delta t$, $\Delta x/\lambda_{De}$ parameter space, was analyzed for the collisionless expansion of a 1-dimensional, sharp-boundary plasma slab into a vacuum. The free expansion of such plasma slabs has been previously discussed by Denavit [5, 8],

including a comparison of particle simulation results to a self-similar solution which assumes charge neutrality, isothermal electrons, and cold ions. As the plasma expands into the vacuum due to the velocity of the particles, a rarefaction wave propagates into the plasma slab at the ion-acoustic speed c_s. The plasma density behind the wavefront falls off exponentially, and the ions are accelerated outward according to the velocity profile

$$v_f = c_s + (x - x_0)/t, \tag{13}$$

where v_f is the velocity of the ions in the rarefaction wave, x_0 is the location of the initial density discontinuity, and x is the location of the ions in the rarefaction at time t. Figure 2 shows the electron and ion phase-space plots for a typical expanding slab. The dashed line on the ion phase-space plot (Figure 2b) represents the self-similar ion front velocity as given by (13). The agreement between the self-similar and particle simulation ion front velocities shown in Fig. 2 was seen earlier in [8].

Freely expanding plasma slab simulations were made for various combinations of

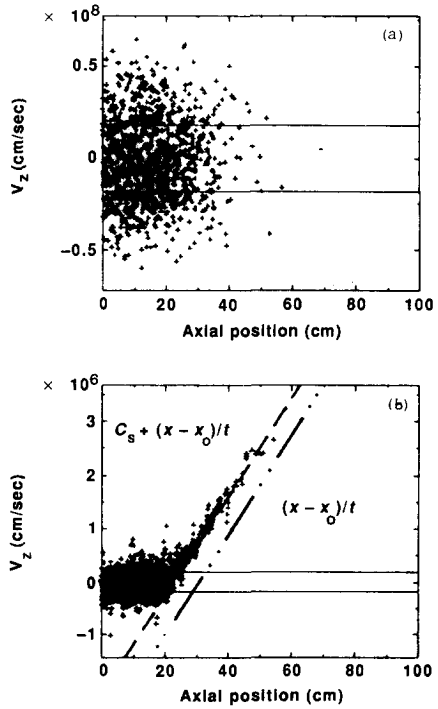

FIG. 2. Phase space distributions for (a) electrons and (b) ions in the freely expanding plasma slab. The initial density discontinuity was located at $x_0 = 30.0$ cm. The ions in the expansion region are accelerated due to the self-electric field. Note the agreement between the self-similar and particle simulation ion front velocities.

the important simulation parameters $\omega_{pe}\,\Delta t$ and $\Delta x/\lambda_{De}$ in the range $0.1 \leqslant \omega_{pe}\,\Delta t \leqslant 200$, $0.1 \leqslant \Delta x/\lambda_{De} \leqslant 100$, excluding the region for which $v_e\,\Delta t/\Delta x > 2$, where $v_e = \sqrt{T_e/m_e}$ is the electron thermal speed. Several input parameters were the same for each of the simulations. These include the number of particles (2048 of each species), the mass ratio ($m_i/m_e = 900$), the temperature ratio ($T_e/T_i = 10$), the system half-width ($L = 100$ cm), the initial plasma slab half-width ($L_{\text{slab}} = 30$ cm) and the mesh size ($\Delta x = L/128 = 0.7843$ cm). The values of ω_{pe} and Δx were the same for each of the simulations, while the temperature of the species (and hence λ_{De}) and Δt were varied.

In an attempt to quantify the performance of the two time integration schemes in various regions of $\omega_{pe}\,\Delta t$, $\Delta x/\lambda_{De}$ parameter space, we employ the quantity $(\Delta E/E_0)/N$, where ΔE is the change in the total plasma energy (kinetic plus electrostatic) through N time steps, normalized to the initial value of total plasma energy E_0. Figure 3 shows a typical time history of the total plasma energy for a simulation that resulted in numerical heating of the plasma. The freely expanding slab should exactly conserve energy, since the kinetic energy of the hot electrons is simply transferred to the cold ions through the self-electric field, resulting in the acceleration of the ions which was observed in Fig. 2b. However, since the implict algorithms described here are inherently dissipative, energy is *not* necessarily conserved. Some possible causes or mechanisms of non-conservation of energy include (i) stochastic self-heating effects [9–11], (ii) self-heating effects arising from the interaction of spatial aliases, which are a consequence of the discrete nature of the grid, with the velocity distribution function of the particles [12], and (iii) numerical heating and cooling due to the dissipative nature of the implicit time integration scheme [2, 13]. This section presents the results of a study of the dependence of energy conservation on $\omega_{pe}\,\Delta t$ and $\Delta x/\lambda_{De}$ using the C_1 and D_1 implicit time integration schemes.

A set of 35 simulations were run for various combinations of $\omega_{pe}\,\Delta t$, $\Delta x/\lambda_{De}$ which span the aforementioned space. These runs were made using the C_1 and D_1 schemes, both with an without one-pass, local, self-consistent digital smoothing of (10) as described in detail in Section 3.3 of Langdon *et al.* [3]. The spatial smoothing that was applied was of a simple, three-point (1, 2, 1) form. It was therefore also possible to study the effect of spatial smoothing on the non-conservation of energy.

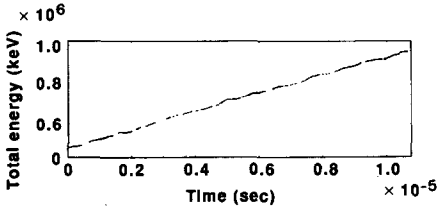

FIG. 3. A typical time history plot of the total plasma energy for a simulation that resulted in numerical heating of the plasma.

The energy conservation results for these runs are given in Tables I and II for the C_1 scheme with and without spatial smoothing and in Tables III and IV for the D_1 scheme with and without smoothing, respectively. The data from these tables is shown in the contour plots of Figs. 4 through 7.

The zero contour line on these figures indicates exact energy conservation, while positive (negative) contour lines indicate numerical heating (cooling) of the plasma. (The positive contour lines are solid, the negative contour lines are dashed, the zero contour line is the bold solid curve and the $v_e \Delta t/\Delta x = 1$ line is the bold dashed line). The filled circles show the locations in $\omega_{pe} \Delta t$, $\Delta x/\lambda_{De}$ parameter space at which the simulations were run. The coarse nature of the contour lines is due to the limited number of runs in the simulation set. The space could be extended to larger values of the two parameters, but the cost of each run increases rapidly as $\Delta x/\lambda_{De}$ is increased, due to the decreasing particle thermal velocity, which in turn requires a greater number of time steps for a uniform expansion of the slab among of all of the runs.

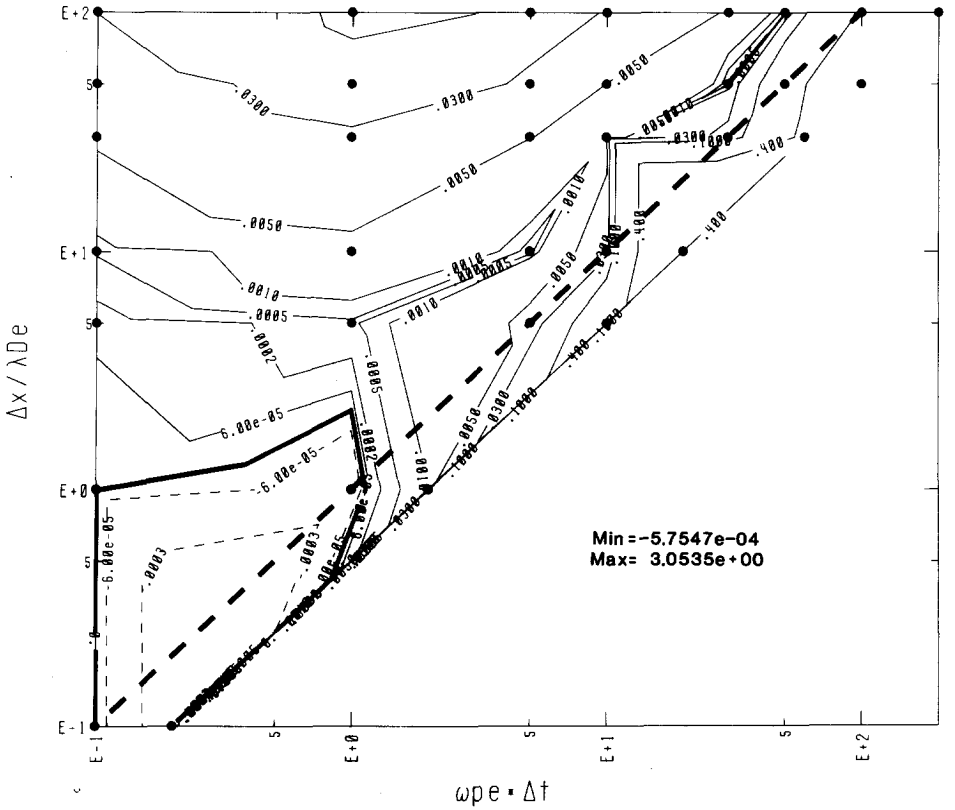

FIG. 4. Contour plots of $(\Delta E/E_0)/N$ as a function of $\omega_{pe} \Delta t$ and $\Delta x/\lambda_{De}$ for the C_1 scheme without spatial smoothing. The zero contour indicates exact conservation of energy.

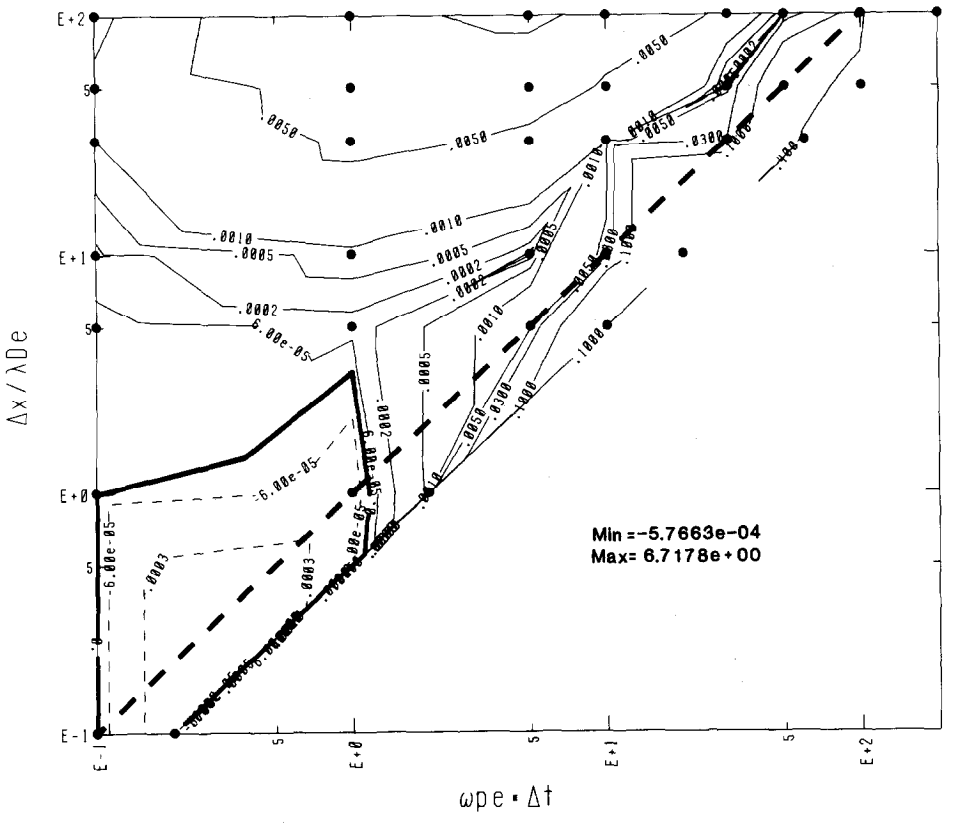

FIG. 5. Contour plots of $(\Delta E/E_0)/N$ as a function of $\omega_{pe}\,\Delta t$ and $\Delta x/\lambda_{De}$ for the C_1 scheme with spatial smoothing. The zero contour indicates exact conservation of energy.

Explicit particle simulation codes are usually limited to operation in the lower left hand region above the bold dashed line [9–11]. The direct implicit method greatly extends this region of operation. The figures indicate that it is possible to use large values of $\omega_{pe}\,\Delta t$ and $\Delta x/\lambda_{De}$ which result in negligible or no loss of energy conservation. Therefore, one may increase the cost effectiveness of the simulation by employing a time step which is larger than the electron plasma period, while accurately simulating the low-frequency phenomena of interest, such as MHD (in implicit electromagnetic codes) and particle transport. It must be stressed that the results presented here are applicable for either periodic plasma systems or systems in which the plasma is not in contact with a wall. The effect of potential sheaths near a surface may yield different conclusions regarding regions of numerical heating and cooling than those presented here.

The contour plots for the C_1 scheme, Figs. 4 and 5, show that energy is conserved up to maximum values of $\Delta x/\lambda_{De} \approx 3$ and $\omega_{pe}\,\Delta t \approx 1$. For larger values of these

TABLE I

Energy Conservation $(\Delta E/E_0)/N$ for the C_1 Scheme without Spatial Smoothing in $\omega_{pe}\,\Delta t$, $\Delta x/\lambda_{De}$ Parameter Space

	$\omega_{pe}\,\Delta t$											
$\Delta x/\lambda_{De}$	0.1	0.2	1.0	2.0	5.0	10.0	20.0	30.0	50.0	60.0	100.0	200.0
100.0	3.1×10^{-2}		1.3×10^{-1}		7.6×10^{-2}	2.3×10^{-2}		2.7×10^{-3}	2.6×10^{-4}		4.5×10^{-1}	3.1×10^{0}
50.0	1.7×10^{-2}		6.6×10^{-2}		1.9×10^{-2}	4.8×10^{-3}		9.7×10^{-5}	2.0×10^{-1}		1.1×10^{0}	
30.0	6.0×10^{-3}		2.3×10^{-2}		5.2×10^{-3}	1.4×10^{-3}		4.0×10^{-2}		4.8×10^{-1}		
10.0	5.4×10^{-4}		2.8×10^{-3}		2.1×10^{-4}	9.6×10^{-3}	1.2×10^{0}					
5.0	9.4×10^{-5}		4.1×10^{-4}		6.3×10^{-3}	2.1×10^{-1}						
1.0	0.0		-1.7×10^{-4}	1.0×10^{-3}								
0.1	0.0	-5.8×10^{-4}										

TABLE II

Energy Conservation $(\Delta E/E_0)/N$ for the C_1 Scheme with Spatial Smoothing in $\omega_{pe}\,\Delta t$, $\Delta x/\lambda_{De}$ Parameter Space

	$\omega_{pe}\,\Delta t$											
$\Delta x/\lambda_{pe}$	0.1	0.2	1.0	2.0	5.0	10.0	20.0	30.0	50.0	60.0	100.0	200.0
100.0	4.7×10^{-4}		2.6×10^{-3}		3.9×10^{-2}	1.5×10^{-2}		2.0×10^{-3}	2.1×10^{-4}		1.5×10^{-1}	6.7×10^{0}
50.0	1.3×10^{-3}		1.1×10^{-2}		1.0×10^{-2}	3.7×10^{-3}		0.0	2.1×10^{-1}		5.7×10^{-1}	
30.0	9.9×10^{-4}		6.6×10^{-3}		3.1×10^{-3}	1.1×10^{-3}		3.3×10^{-2}		4.3×10^{-1}		
10.0	1.5×10^{-4}		7.9×10^{-4}		2.5×10^{-5}	6.0×10^{-3}	3.8×10^{-1}					
5.0	2.2×10^{-5}		9.2×10^{-5}		1.9×10^{-3}	3.1×10^{-1}						
1.0	0.0		-1.2×10^{-4}	5.6×10^{-4}								
0.1	0.0	-5.8×10^{-4}										

TABLE III

Energy Conservation $(\Delta E/E_0)/N$ for the D_1 Scheme without Spatial Smoothing in $\omega_{pe}\Delta t$, $\Delta x/\lambda_{De}$ Parameter Space

	$\omega_{pe}\Delta t$											
$\Delta x/\lambda_{De}$	0.1	0.2	1.0	2.0	5.0	10.0	20.0	30.0	50.0	60.0	100.0	200.0
100.0	3.2×10^{-2}		1.5×10^{-1}		2.4×10^{-2}	5.7×10^{-3}		-2.0×10^{-4}	-1.5×10^{-3}		-4.3×10^{-3}	-2.2×10^{-3}
50.0	1.6×10^{-2}		3.2×10^{-2}		5.0×10^{-3}	8.7×10^{-4}		-1.6×10^{-3}	-2.7×10^{-3}		-2.4×10^{-3}	
30.0	5.2×10^{-3}		1.2×10^{-2}		1.2×10^{-3}	-5.7×10^{-5}		-3.5×10^{-3}		-2.2×10^{-3}		
10.0	5.4×10^{-4}		1.2×10^{-3}		-7.3×10^{-4}	-3.0×10^{-3}	-6.9×10^{-3}					
5.0	7.9×10^{-5}		0.0		-1.9×10^{-3}	-4.3×10^{-3}						
1.0	-5.2×10^{-6}		-7.8×10^{-4}	-2.0×10^{-3}								
0.1	0.0	-7.5×10^{-4}										

TABLE IV

Energy Conservation $(\Delta E/E_0)/N$ for the D_1 Scheme with Spatial Smoothing in $\omega_{pe}\Delta t$, $\Delta x/\lambda_{De}$ Parameter Space

	$\omega_{pe}\Delta t$											
$\Delta x/\lambda_{De}$	0.1	0.2	1.0	2.0	5.0	10.0	20.0	30.0	50.0	60.0	100.0	200.0
100.0	4.8×10^{-4}		9.5×10^{-3}		8.9×10^{-3}	4.0×10^{-3}		-2.4×10^{-4}	-1.4×10^{-3}		-4.3×10^{-3}	-2.5×10^{-3}
50.0	1.3×10^{-3}		5.8×10^{-3}		3.0×10^{-3}	7.7×10^{-4}		-1.7×10^{-3}	-2.7×10^{-3}		-3.2×10^{-3}	
30.0	9.5×10^{-4}		2.8×10^{-3}		6.8×10^{-4}	-1.6×10^{-4}		-3.5×10^{-3}		-2.7×10^{-3}		
10.0	1.6×10^{-4}		2.4×10^{-4}		-8.0×10^{-4}	-3.1×10^{-3}	-7.1×10^{-3}					
5.0	2.0×10^{-5}		-7.4×10^{-5}		-1.9×10^{-3}	-5.1×10^{-3}						
1.0	0.0		-7.0×10^{-4}	-2.1×10^{-3}								
0.1	0.0	-7.5×10^{-4}										

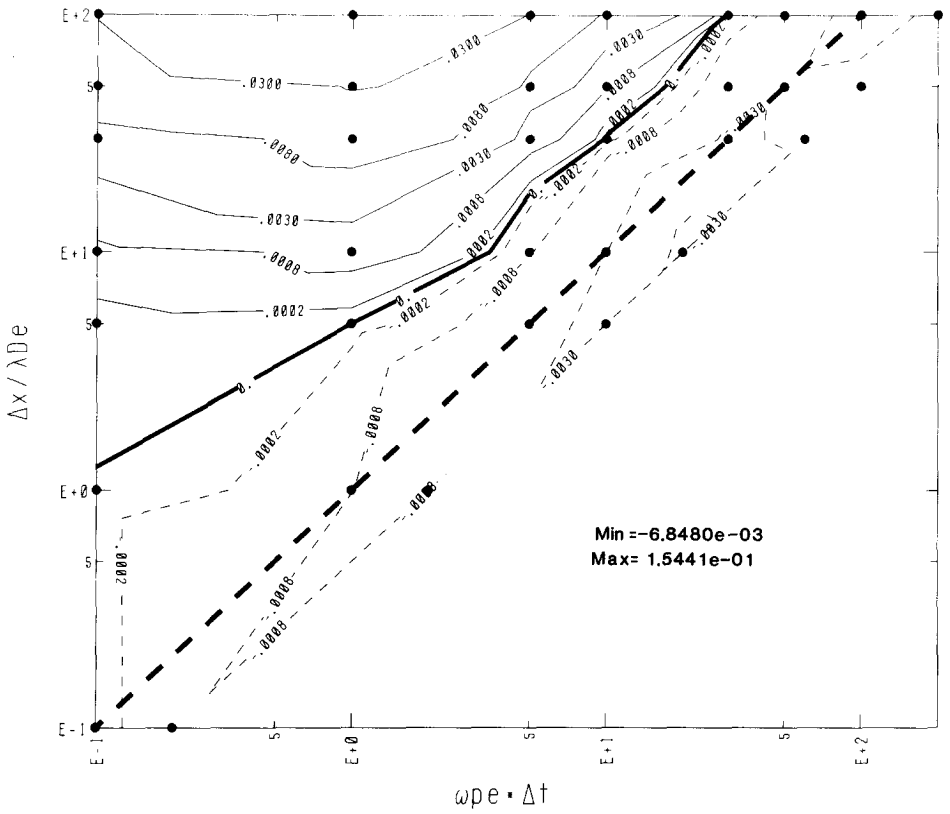

FIG. 6. Contour plots of $(\Delta E/E_0)/N$ as a function of $\omega_{pe}\,\Delta t$ and $\Delta x/\lambda_{De}$ for the D_1 scheme without spatial smoothing. The zero contour indicates exact conservation of energy.

parameters, there is numerical heating, while smaller values lead to numerical cooling of the plasma. The addition of local spatial smoothing allows the zero contour line to extend to slightly larger values of the two parameters. Smoothing also reduces the numerical heating at large values of $\Delta x/\lambda_{De}$ by about a factor of 4. The data points at $\omega_{pe}\,\Delta t = 200$, $\Delta x/\lambda_{De} = 100$ are subject to very rapid numerical heating with the C_1 scheme. Spatial smoothing increases the heating rate at this point, which is the opposite effect to that seen in other regions of the parameter space.

In contrast to the contour plots for the C_1 scheme, Figs. 6 and 7 indicate that there are regions in the space with large values of $\omega_{pe}\,\Delta t$ and $\Delta x/\lambda_{De}$ for which the energy of the system is conserved well when the D_1 scheme is used. The zero contour line lies approximately parallel to the $v_e\,\Delta t/\Delta x = 1$ (bold dashed) line, and extends out to $\omega_{pe}\,\Delta t \approx 30$, $\Delta x/\lambda_{De} = 100$ following a path described approximately by $v_e\,\Delta t/\Delta x \approx 0.3 \pm 0.1$ for $\omega_{pe}\,\Delta t \gtrsim 1$, $m_i/m_e = 900$, and $T_e/T_i = 10$. This behavior may continue to larger values of the two parameters, which would allow for very large time step simulations in which numerical heating and cooling are not signifi-

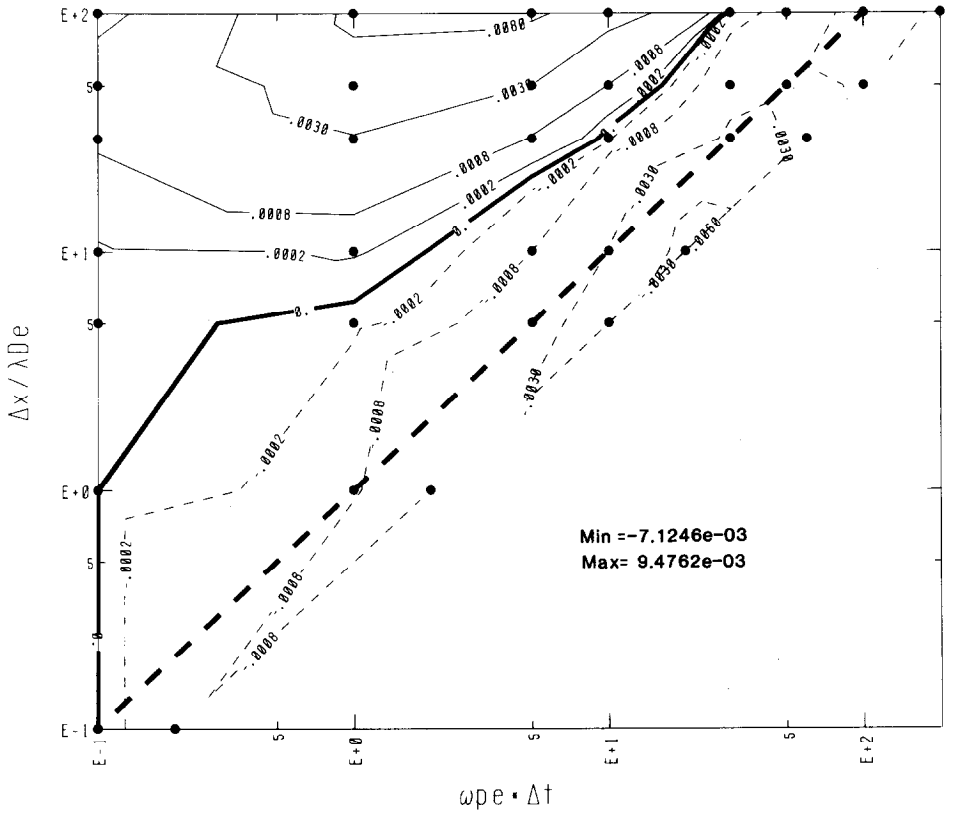

FIGURE 7. Contour plots of $(\Delta E/E_0)/N$ as a function of $\omega_{pe}\Delta t$ and $\Delta x/\lambda_{De}$ for the D_1 scheme with spatial smoothing. The zero contour indicates exact conservation of energy.

cant. Note that there is a very rapid rate of change in $(\Delta E/E_0)/N$ about the zero contour line, especially for $\omega_{pe}\Delta t \gtrsim 1$. Spatial smoothing yields approximately a factor of 5 reduction in the numerical heating at large values of $\Delta x/\lambda_{De}$.

4. NONLINEAR INSTABILITY

To this point we have been concerned with the performance (specifically energy conservation) of the direct implicit scheme in a rather idealized environment. We have tested several schemes in anticipation of the need to increase time step and reduce grid resolution as our interests turn to larger problems and higher dimensionality. Another concern is that the algorithm would become less robust or perhaps nonlinearly unstable when attempting to simulate plasmas with large fluctuations due to few particles per cell—a strong temptation as problem requirements increase.

Now we report experiments with several variants of the scheme in an effort to determine the limitations as the plasma representation becomes more coarse, with the aim of isolating those forms most suitable for extension to a 2-dimensional, electromagnetic code. In the work reported here, we selected a number of the simpler, though less rigorously justified, algorithms. Most of the variants were eliminated by tests on the same expanding slab problem, which features initially sharp gradients, a large range of density, and parameters that stress the linearization on which the field predictor is based. Local fluctuations are frequently the cause of such stress due to the large fields produced by motion of isolated, individual particles representing too many real particles. Such situations may occur when too few particles per cell N_c are used and always occur in regions of low density near a sharp plasma gradient. The surviving algorithms are as simple as any that have been proposed, yet are (so far) more robust than we expected.

Our tests used values of $\omega_{pe}\,\Delta t$ as large as 200, much larger than have been reported previously [14, 15, 5]. With the larger values of $\omega_{pe}\,\Delta t$, some algorithms exhibited nonlinear numerical instability when $(\omega_{pe}\,\Delta t)^2$ exceeded N_c, where N_c is the number of particles per cell (in one dimension, $N_c = n\,\Delta x$). Many applications of 2-dimensional explicit codes require only that $N_c \gtrsim 10$. If the nonlinear instability were not circumvented, we would need more than $(\omega_{pe}\,\Delta t)^2$ particles per cell, which would be a severe limitation.

In this section we detail the method that works best and explain why other variants are less robust.

Several suitable schemes for time-differencing the particles have been analyzed and applied [2]. We consider only the "D_1" scheme, here written as

$$\frac{\mathbf{x}_{n+1} - \mathbf{x}_n}{\Delta t} = \mathbf{v}_{n+1/2} \tag{14a}$$

$$\frac{\mathbf{v}_{n+1/2} - \mathbf{v}_{n-1/2}}{\Delta t} = \bar{\mathbf{a}}_n + \frac{\mathbf{v}_{n+1/2} + \mathbf{v}_{n-1/2}}{2} \times \frac{q\mathbf{B}_n}{mc}, \tag{14b}$$

where

$$\bar{\mathbf{a}}_n = \tfrac{1}{2}[\bar{\mathbf{a}}_{n-1} + \mathbf{a}_{n+1}], \tag{15}$$

$\mathbf{a}$ is the acceleration due to the electric field only, and n is the time level. The variables $\mathbf{x}$, $\mathbf{v}$, and $\mathbf{a}$ are quantities associated with each particle.

The direct-implicit method is used here in the following 1-dimensional, unmagnetized, electrostatic algorithm. The position $\mathbf{x}_{n+1}$ of a particle at time level t_{n+1}, as given by (14), can be written as Eq. (4) with $\beta = \frac{1}{2}$ for the D_1 scheme, and $\tilde{x}_{n+1}$ is the position obtained from the equation of motion with the acceleration a_{n+1} omitted; $\tilde{x}_{n+1} = x_n + v_{n-1/2}\,\Delta t + \frac{1}{2}\bar{a}_{n-1}\,\Delta t^2$ is known in terms of positions, velocities, and accelerations at times t_n and earlier. In its simplest form, which we adopt here, the direct implicit algorithm is derived by linearization of the particle positions relative to $\tilde{x}_{n+1}$.

At the grid point located at X_j, the charge density $\tilde{\rho}_{j,n+1}$ is formed by adding the contributions of the simulation particles at positions $\{\tilde{x}_{i,n+1}\}$ interpolated to the mesh,

$$\tilde{\rho}_{j,n+1} = \sum_i q_i S(X_j - \tilde{x}_{i,n+1}), \tag{16}$$

where $X_j \equiv j\,\Delta x$, Δx is the grid spacing, i is the particle index, q_i is the charge, and S is the particle-grid interpolation spline. With this extrapolated charge density and the linearized implicit contribution $-\partial(\chi E)/\partial x$, the field equation can be written in the form of (11) or as

$$\tilde{\rho}_{j,n+1} = [(1+\chi_{j+1/2})\,E_{j+1/2,n+1} - (1+\chi_{j-1/2})\,E_{j-1/2,n+1}]/\Delta x, \tag{17}$$

where $\chi(\mathbf{x}) = \sum \beta\tilde{\rho}(\mathbf{x})(q/m)\,\Delta t^2$ summed over species, i.e., $\chi = \beta(\omega_p\,\Delta t)^2$. We call χ the implicit susceptibility, because of the similarity of (11) and (17) to the field equation in nonuniform dielectric media. Note that $\chi \gg 1$, where $\omega_p\,\Delta t$ is large. The two representations used here are (12) and

$$\chi_{j+1/2} = \max(\chi_j, \chi_{j+1}), \tag{18}$$

where

$$\chi_j = \Delta t^2 \sum_s \left[\beta\tilde{\rho}_{j,n+1}\frac{q}{m}\right] \tag{19}$$

is a sum over species index s.

In terms of the field

$$E_{j,n+1} = \tfrac{1}{2}[E_{j-1/2,n+1} + E_{j+1/2,n+1}] \tag{20}$$

formed from values of E at the half-integer positions, the particle acceleration is evaluated at $\tilde{x}_{n+1}$ by an interpolation of the form

$$m_i a_{i,n+1} = q_i\,\Delta x \sum_j E_{j,n+1} S(X_j - \tilde{x}_{i,n+1}), \tag{21}$$

where the sum is over grid points j and S is the same spline function used in (16). (We have chosen not to include spatial smoothing, because the resulting loss of resolution may be too costly in two dimensions and because smoothing makes the field equation more expensive to solve.)

Two parameters measure the stress on the algorithm: The more important parameter is $\chi_1 = \beta q^2\,\Delta t^2/m\,|\Delta x|$, where q and m are the particle charge and mass, and $|\Delta x|$ is the zone volume. This is a worst-case measure of the validity of linearization in the field prediction, as stressed by short-wavelength sampling fluctuations in the charge density. Written as $\beta(\omega_{pe}\,\Delta t)^2/N_c$, this parameter, χ_1, is seen to be greater than unity when $\beta(\omega_{pe}\,\Delta t)^2 > N_c$; its significance is mentioned above.

The second parameter is $v_e \Delta t/\Delta x$, the ratio of thermal electron transit distance per cycle to the zone size. Although a direct-implicit code is stable with $v_e \Delta t/\Delta x > 1$, energy conservation is degraded without use of spatial smoothing.

Depending on the differencing of the field equation, the ratio $(x_{n+1} - \tilde{x}_{n+1})/\Delta x$, a measure of the validity of linearization in the absence of smoothing, can be as large as $\beta \Delta t^2 (q^2/m)/|\Delta x| = \chi_1$ due to the field of a *single* particle, in regions of large density gradient or low density. It is essential that a particle contribute enough to the χ's multiplying all the $\{E_{j+1/2}\}$ that accelerate the particle and its neighbors in the same zone, so that the χ's are big enough to ensure that the electric fields and, hence, the accelerations do not become too large. The choices (12) and (18) work well in the test problems considered. However, in the momentum conserving algorithm [16; 13, Section II.C.2], the formation of χ must be more "local" than it is in (12) and (18) (that is, a particle must contribute to fewer χ's). With algebraic momentum conservation in any form attractive for extension to two dimensions and electromagnetic fields (i.e., using neither spatial filtering, iteration, nor "strict" formulations of the field predictor (in the sense given in [1; 2])), we have not been able to run with $\chi_1 \gtrsim 1$. When these simulations fail, electric fields become large typically in the regions of low density: particles are accelerated to high energies and can cross many cells in one time step.

With the formulation outlined here, we have obtained reasonable results with χ_1 well over 100, which considerably reduces the required number of particles per cell when $(\omega_{pe} \Delta t)^2$ is large. In Table V we summarize the numerical results for a series of simulations testing nonlinear stability using the D_1 scheme with simplified differencing and $\chi_{j+1/2}$ given by Eq. (12). The simulations uniformly cool and remain stable for all values of χ_1 used, $0.0125 \leqslant \chi_1 \leqslant 20$. The cooling observed here is qualitatively consistent with the results at different values of χ_1 shown earlier in Fig. 6 for $\Delta x/\lambda_{De} = 2\omega_{pe} \Delta t$, which data follows a contour lying below the solid line along which energy is conserved.

TABLE V

Energy Conservation $(\Delta E/E_0)/N$ for the D_1 Scheme without Spatial Smoothing in $\omega_{pe} \Delta t$, $\Delta x/\lambda_{De}$, and χ_1 Parameter Space

	$\omega_{pe} \Delta t = \Delta x/(2\lambda_{De})$		
χ_1	0.2	2.0	20.0
20.0		-1.3×10^{-3}	-6.9×10^{-3}
2.0	-3.1×10^{-4}	-1.5×10^{-3}	-7.7×10^{-3}
1.25		-1.4×10^{-3}	-7.5×10^{-3}
0.2	-1.8×10^{-4}	-9.6×10^{-4}	
0.125		-7.1×10^{-4}	-7.4×10^{-3}
0.0125	-9.8×10^{-5}	-2.7×10^{-4}	

5. Summary

The C_1 and D_1 direct implicit time integration schemes have been shown to extend the region of operation for which the total plasma energy is conserved beyond that which is applicable for an explicit time integration scheme. The C_1 scheme was found to have a limited region of parameter space over which energy is well conserved. The D_1 scheme possesses a much larger region of parameter space for good energy conserving operation. In fact, for the range of parameter space considered, the D_1 scheme was shown to conserve energy well along a path described by $v_e \Delta t/\Delta x \sim 0.3$. This guideline has served well in 2-dimensional electromagnetic applications of AVANTI [7] for a wide range of parameters. Numerical heating was found for large values of $\Delta x/\lambda_{De}$ with each of the schemes. The amount of heating in a given region of the space was found to be comparable between the two schemes, with the D_1 scheme heating slightly less than the C_1 scheme. Numerical cooling of the plasma system was found for the lowest values of the parameters in the space, except when the D_1 scheme was used with local spatial smoothing. Spatial smoothing generally yielded a factor of 3 to 4 reduction in the amount of numerical heating, and a slight decrease in the amount of numerical cooling relative to the same simulation run without smoothing. The smoothing did not substantially alter the gross topology of the energy conservation plots.

We note with interest that the guideline of $v_e \Delta t/\Delta x \sim 0.3$ for the direct implicit algorithm falls in the middle in the range $O(10^{-1}) < v_e \Delta t/\Delta x < O(1)$ determined empirically by Brackbill and Forslund [17] in order that the implicit moment method for particle simulation gives stable and accurate results. Brackbill and Forslund found that the lower limit is associated with the onset of the finite grid instability and the upper limit results from the deterioration of the accuracy of the particle trajectories.

If low-frequency phenomena are of interest, as opposed to high-frequency effects, the large degree of high-frequency damping provided by the D_1 scheme (see Fig. 1) allows the use of time steps that encompass several electron plasma periods. The $\omega_{pe} \Delta t$ time step constraint is thereby relaxed, resulting in an increased cost effectiveness of the simulation. For such simulations, the D_1 scheme is more desirable for use than the C_1 scheme. Since the energy conservation contour plot for the D_1 scheme has a steep gradient about the energy conserving contour, care must be taken to ensure that the operation point is chosen as close to the energy conserving contour as possible.

Code experience with C_1 and D_1 time differencing schemes, with strict and simplified spatial differencing [18], and with and without momentum conservation [16, 18] also indicates that some forms of the direct implicit algorithms are susceptible to a nonlinear numerical intability that can occur when $(\omega_{pe} \Delta t)^2$ exceeds the number of particles in a cell. However, algorithms with simplified spatial differencing and without momentum conservation do not exhibit the nonlinear instability for values of $(\omega_{pe} \Delta t)^2$ greatly exceeding the number of particles in a cell. Hence, we advocate use of the D_1 scheme with simplified spatial differencing as described here

in Section 4. This is being successfully pursued in 2-dimensional electromagnetic applications [7].

ACKNOWLEDGMENTS

We are grateful to A. Friedman and C. K. Birdsall for their assistance and encouragement in this research. The research of R. J. Procassini was partially supported through the Plasma Physics Research Institute of the University of California at Lawrence Livermore National Laboratory. This work was performed under the auspices of the U.S. Department of Energy by the Lawrence Livermore National Laboratory under Contract W-7405-Eng-48.

REFERENCES

1. A. B. LANGDON, *J. Comput. Phys.* **30**, 202 (1979).
2. B. I. COHEN, A. B. LANGDON, AND A. FRIEDMAN, *J. Comput. Phys.* **46**, 15 (1982).
3. A. B. LANGDON, B. I. COHEN, AND A. FRIEDMAN, *J. Comput. Phys.* **51**, 107 (1983); B. I. COHEN, A. B. LANGDON, AND A. FRIEDMAN, *J. Comput. Phys.* **56**, 51 (1984).
4. R. J. MASON, *J. Comput. Phys.* **41**, 223 (1981).
5. J. DENAVIT, *J. Comput. Phys.* **42**, 337 (1981).
6. A. B. LANGDON AND D. W. HEWETT, in *Proceedings, Twelfth Conf. Num. Sim. Plasmas, San Francisco, CA, September 20–23, 1987*, PT17.
7. D. W. HEWETT AND A. B. LANGDON, *J. Comput. Phys.* **72**, 121 (1987).
8. J. DENAVIT, *Phys. Fluids* **22**, 1384 (1979).
9. R. W. HOCKNEY, *J. Comput. Phys.* **8**, 19 (1971).
10. A. PEIRAVI AND C. K. BIRDSALL, in *Proceedings, Eighth Conf. Num. Sim. Plasmas, Monterey, CA, June 28–30, 1978*, PD-9.
11. C. K. BIRDSALL AND A. B. LANGDON, *Plasma Physics via Computer Simulation* (McGraw–Hill, New York, 1985), p. 293.
12. A. B. LANGDON, *J. Comput. Phys.* **6**, 247 (1970).
13. A. B. LANGDON AND D. C. BARNES, "Direct Implicit Plasma Simulation," in *Multiple Time Scales*, Computational Techniques (Academic Press, New York, 1985), p. 335.
14. H. SAKAGAMI, K. NISHIHARA, AND D. COLOMBANT, Institute of Laser Engineering Research Report ILE8117P, Osaka University, August 10, 1981 (unpublished).
15. A. FRIEDMAN, A. B. LANGDON, AND B. I. COHEN, *Laser Program Annual Report-1982*, Lawrence Livermore National Laboratory, Livermore, CA, UCRL-50021-82, 1983, p. 3 (unpublished).
16. A. FRIEDMAN AND B. I. COHEN, in *Proceedings, Tenth Conf. Num. Sim. Plasmas, San Diego. CA, January 4–6 1983*, 2A-3.
17. J. U. BRACKBILL AND D. W. FORSLUND, *J. Comput. Phys.* **46**, 271 (1982).
18. A. B. LANGDON, D. W. HEWETT, AND A. FRIEDMAN, *Laser Program Annual Report-1983*, Lawrence Livermore National Laboratory, Livermore, CA, UCRL-50021̄83, 1983, p. 3 (unpublished).